

A Double Scattering Analytical Model For Elastic Recoil Detection Analysis

N. P. Barradas ^{1,2}, K. Lorenz ^{1,2}, V. Darakchieva ^{1,2,3}, E. Alves ^{1,2}

⁽¹⁾ Instituto Tecnológico e Nuclear, E.N. 10, Sacavém 2686-953, Portugal

⁽²⁾ Centro de Física Nuclear da Universidade de Lisboa, Av. Prof. Gama Pinto 2, 1649-003 Lisboa, Portugal

⁽³⁾ IFM, Linköping University, SE-581 83 Linköping, Sweden

Abstract. We present an analytical model for calculation of double scattering in elastic recoil detection measurements. Only events involving the beam particle and the recoil are considered, i.e. 1) an ion scatters off a target element and then produces a recoil, and 2) an ion produces a recoil which then scatters off a target element. Events involving intermediate recoils are not considered, i.e. when the primary ion produces a recoil which then produces a second recoil. If the recoil element is also present in the stopping foil, recoil events in the stopping foil are also calculated. We included the model in the standard code for IBA data analysis NDF, and applied it to the measurement of hydrogen in Si.

Keywords: double scattering; ERDA; indium nitride

PACS: 82.80.Yc; 81.05.Ea; 02.60.Cb

INTRODUCTION

Data analysis of techniques such as Rutherford backscattering (RBS) or elastic recoil detection (ERDA) relies on accurate simulations of the spectra expected for a given sample structure. In complex cases, effects such as plural and multiple scattering have to be taken into account [1,2], and analytical calculations to simulate those effects are often not available.

In Monte Carlo simulations (MC), in principle, all effects can be included, including the exact geometrical configuration of the detection system [3,4]. In practice, the calculations can be very slow, and so-called acceleration techniques [3,5,6] have been developed to increase the efficiency of the calculations. These include using in the MC simulations virtual (larger) detectors, restricting the possible scattering angles, and artificially increasing the mean free paths of the beam particles. This means that what one calculates is not necessarily equivalent to what one measures, particularly at low energies where the very high cross sections make MC unpractical, and at very grazing angles where the acceleration techniques can lead to strong distortions in the calculations. Nevertheless, MC methods have proven very successful in making detailed calculation of plural and multiple scattering effects [7]. However, even if the codes are in principle available, practically

all the publications involving MC have been made by the authors of the codes. The recent development of a user friendly Windows interface for the MC code Corteo [6] is however bound to increase its usage.

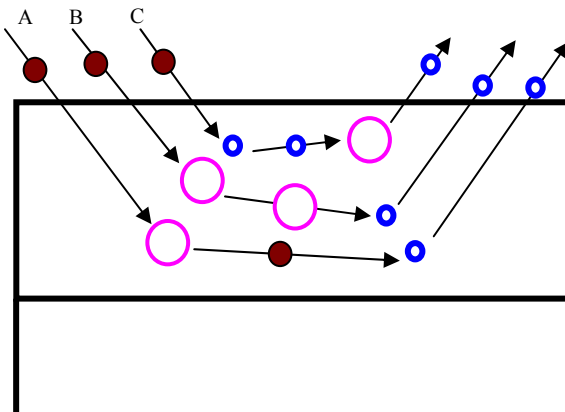


FIGURE 1. Double scattering trajectories in ERDA. The figure represents the target film..Full circles represent the primary ion. Small open circles represent the detected recoil. Large open circles represent a target atom other than the recoil.

Nevertheless, MC simulation is still not appropriate for widespread routine data analysis, for which analytical codes continue to be the first choice. Improving the quality of the analytical simulations is

thus essential. Double scattering (DS), which is the simplest particular case of plural scattering, leads to a low energy background which, in RBS, decreases the sensitivity to low Z elements present in the sample. In ERDA, it reduces the sensitivity to the presence of the recoil atom in deeper layers. We have previously developed an analytical model of double scattering for RBS [8]. We now extended it to ERDA, and included it in the code NDF [9,10]. Here we give details of the calculation method, and show its relevance in the measurement of hydrogen in Si and in indium nitride with ${}^4\text{He}$ -ERDA.

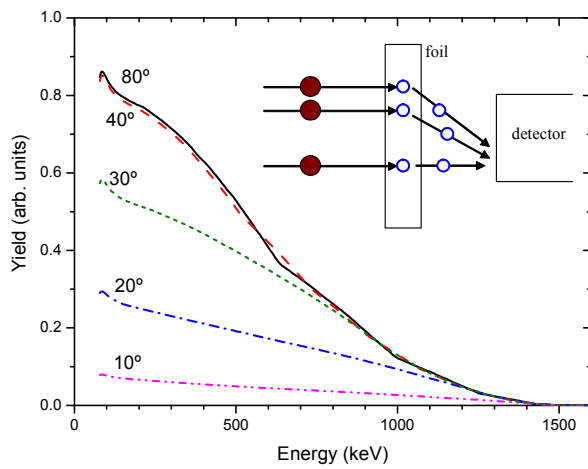


FIGURE 2. Contribution of production of recoils in the stopping foil for a 165 nm thick $\text{SiH}_{0.20}$ target film on Si. A $1.25 \times 1020 \text{ at./cm}^2$ Mylar stopping foil is considered. Each curve is for one maximum value of the recoil angle in the stopping foil. The insert shows the geometry and different possibilities. Clearly, the result will depend on the exact dimensions of stopping foil and detector and distance between them. Large open circles represent a target atom other than the recoil.

DOUBLE SCATTERING MODEL

The first analytical calculations of DS in RBS were presented by Weber et al. [11]. They considered only normal incidence, and imposed a minimum scattering angle $\alpha_{\min}=15^\circ$. The Rutherford cross section is not defined for a 0° scattering angle, and it has only been experimentally verified for scattering angles down to 15° [12]. Eckstein and Mayer generalised the algorithm to any geometry [13], using 120 solid angle intervals (i.e. for the direction of the beam after the first scatter event), and $\alpha_{\min}=20^\circ$, obtaining good agreement with experiments made close to normal incidence. Barradas [8] showed that the concept of a minimum scattering angle is not appropriate in grazing angle geometry, because small changes in angle can

lead to large changes in the actual trajectory of the ions. Instead, one must consider the deviation of each trajectory from the corresponding single scattering trajectory. The resulting algorithm leads to excellent results in grazing angle RBS, where DS can be very large. If one imposes instead α_{\min} around 20° , a calculated low energy background with approximately the correct shape is obtained, but one order of magnitude too low. This is relevant for ERDA, which is usually made in grazing angle geometry.

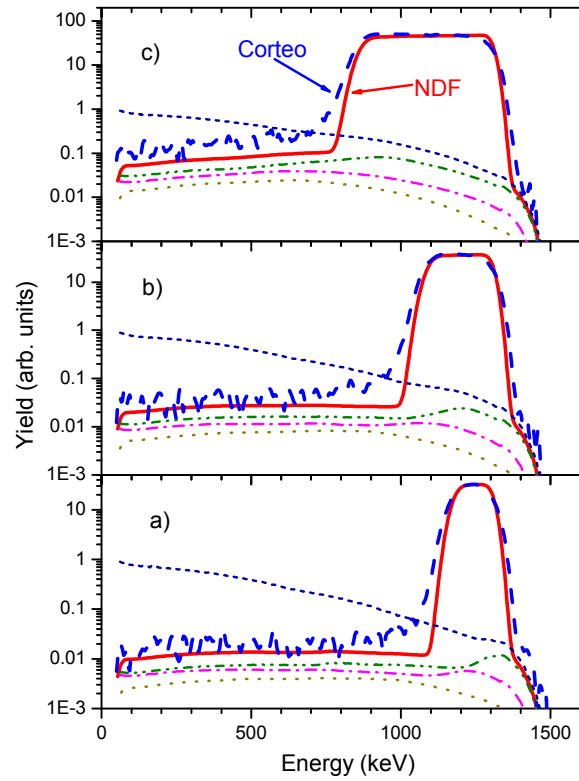


FIGURE 3. Calculations for target films on Si: a) 165 nm $\text{SiH}_{0.20}$, b) 275 nm $\text{SiH}_{0.23}$, c) 550 nm $\text{SiH}_{0.30}$. Thick solid and dashed lines are the NDF and Corteo calculations. Dash-dotted and dash-dot-dotted are the contributions of trajectories of type A and C, as calculated with NDF. The short dashed lines are the contribution of production of recoils in the Mylar stopping foil. The dotted lines are the NDF calculations imposing a hard 20° cut-off angle.

Repllinger et al. presented an analytical calculation for ERDA, where α_{\min} was calculated for each incident ion/target pair on the grounds of an analogy between nuclear and electronic energy loss [14]. It is not stated in the paper how many different solid angle intervals were calculated. They included in the calculations recoils produced by forward scattered primary beam ions in the stopping foil used to prevent the primary ${}^4\text{He}$ beam to reach the detector, which also contained

hydrogen. The low energy background thus calculated had approximately the correct shape, but it was 6 to 20 times smaller than the observed background, for SiH_x target films of thickness between 165 and 550 nm on Si and x between 0.2 and 0.3.

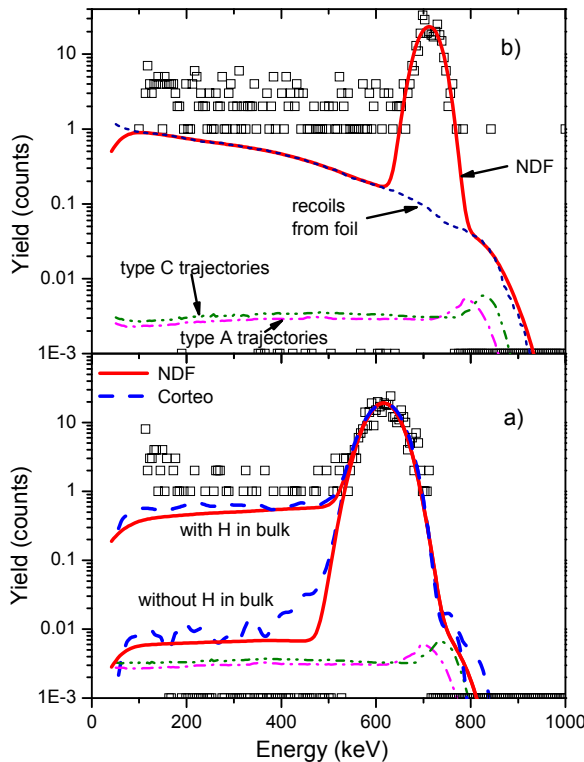


FIGURE 4. Data (squares) collected from the same Si sample, with a) aluminium stopping foil and b) Kapton stopping foil. The lower and upper thick solid and dashed lines in a) are the NDF and Corteo calculations without H in the bulk and with 0.06 at.% H in the bulk. The thick solid line in b) is the NDF calculation assuming no H in the bulk. Dash-dotted and dash-dot-dotted are the contributions of trajectories of type A and C, as calculated with NDF. The short dashed line in b) is the contribution of production of recoils in the stopping foil calculated with NDF.

We extended the DS algorithm previously developed for RBS [8] to ERDA. The algorithm is general, without any restrictions on incident beam, detected particle, number of elements and of layers in the target, or detection geometry. The three main changes towards the RBS algorithm are the following:

1. In RBS, it is the same ion that undergoes the two scattering events. In ERDA, as shown in Fig. 1, there are different possibilities. In trajectory A, a primary beam ion is scattered off a target atom, and then proceeds to create the recoil which is detected. In trajectory B, the primary ion creates an intermediate recoil, different from the detected particle, and the

intermediate recoil then creates the recoil which is detected. In C, the primary ion creates the recoil, which then scatters off a target atom before being detected. We consider only cases A and C, i.e., we ignore case B where two consecutive recoils are produced. The ERDA cross section is only high for large recoil angles, for which the kinematic factor is low; for small recoil angles, the kinematic factor is high but the cross section is low. That is, two consecutive recoil events lead with high probability to a final recoil with energy too small to be detected; conversely, they only lead to a final recoil with energy high enough to be detected with very small probability.

2. The recoil cross section is strongly dependent on the scattering angle. For ${}^4\text{He}$ on hydrogen, the cross section deviates strongly from Rutherford. Furthermore, in events of type C, where the recoil is scattered off target atoms, if the recoil is hydrogen, the cross section for scattering on light elements is almost always very strongly non-Rutherford, with a strong angular dependence. The algorithm developed considers all this, by introduction of cross section tabular data on angle and energy for each reaction. Many of the most used cross sections are included in NDF, and it is easy to introduce new ones as needed, particularly with SigmaCalc and IBANDL [15].

3. Production of recoils in the stopping foil by forward scattered ions is also calculated. However, consider the insert of Fig. 2. It is clear that, depending on the exact geometrical configuration of the stopping foil and of the detector, and distance between them, different angles of scattering in the stopping foil can lead to the detection of particles. An integration on the recoil angle must be made, which depends on the set-up used, and on the exact configuration of any slits that may exist. Fig. 2 shows the calculated contribution to DS of recoils produced in the stopping foil, for a 165 nm thick $\text{SiH}_{0.2}$ target film on Si measured with 2.9 MeV ${}^4\text{He}$ and a 1.25×10^{20} at./ cm^2 Mylar ($\text{C}_{10}\text{O}_4\text{H}_8$) stopping foil, for different maximum recoil angles, assuming scattering in a cone around the nominal beam direction, which is an ideal situation that real set-ups often do not match. Up to 40° , there is a fast increase of the calculated DS yield, which then stabilises because recoils produced in the stopping foil at a larger angle are stopped within the stopping foil itself.

RESULTS AND DISCUSSION

We show in Fig. 3 calculations corresponding to three SiH_x target films: 165 nm with $x=0.2$, 275 nm with $x=0.23$, and 550 nm with $x=0.3$, measured with 2.9 MeV ${}^4\text{He}$ and a 1.25×10^{20} at./ cm^2 Mylar stopping

foil, that is, corresponding to what Repplinger et al. showed in Fig. 2 of [14]. Angle-dependent non-Rutherford cross sections were used for ${}^4\text{He}$ on ${}^1\text{H}$ [16], and ${}^1\text{H}$ on Si [17] and on hydrogen [18].

Some of the NDF calculations presented in Fig. 3 do not include the recoils produced in the stopping foil, in order to compare with simulations made with the MC code Corteo [6] (we note that Corteo, in its current version, does not calculate recoils produced in the stopping foil), where 1×10^8 trajectories were calculated without acceleration techniques. In general terms, the NDF and Corteo simulations are very close; the width of the signal calculated with Corteo is slightly larger, and there are some extra counts on the low energy side of the large hydrogen signal. These effects are due to multiple scattering, as shown previously for RBS [1]. More importantly, the shape of the DS background calculated with NDF is very close to Corteo. Quantitatively, the yield calculated with NDF is too small, as the MC simulation is larger by a factor up to 2. This is due to events that involve more than two large angle collisions, that is, plural scattering with 3, 4, 5, or more scattering events [1], that are not included in the NDF dual scattering calculation.

We also show in Fig. 3 the contribution to DS of type A and type C trajectories, as well as the contribution due to recoils produced in the stopping foil with a maximum angle of 40° . We note that, even if we included all the contributions due to DS, by adding the Corteo result with the NDF stopping foil results, the simulated yield (not shown here) would still be much smaller than the data reported in ref. [14]. This can be due to some effect not included in the simulations shown here, but it can also be due to roughness of the samples analysed or even to actual diffusion of hydrogen to the Si substrate.

A Si sample was measured using a 2 MeV ${}^4\text{He}$ beam in consecutive days, in different spots in order to ensure that hydrogen loss, if it occurs, during the experiment was not affecting the measurement. The only difference between the two measurements is that on one day the stopping foil was Kapton, and on the next day it was Al. The data are shown in Fig. 4. We first consider the simulations made with NDF assuming that hydrogen is only present in the surface; for both stopping foils the calculated yield at energies lower than the surface peak is below the observed data. Believing that the simulations are actually correct, this would mean that a sub-surface layer around 300 nm thick has a small hydrogen content, with 0.06 at.% leading to a calculated integrated low energy yield equal to the experimental data collected with the Al stopping foil (see Fig. 4). A concentration of hydrogen in the stopping foil around 8 at.% would be needed to explain the data, which is not realistic.

We note however that we cannot exclude effects such as scattering in the chamber, in the slits, in the detector aperture, or even electronics noise in the system, that might lead to the observed background. The 0.06 at.% must then be taken as the maximum hydrogen concentration below the surface. The sensitivity to hydrogen in the bulk is much better with the Al stopping foil, on the one hand because of the smaller background, and on the other hand due to the difficulties in the calculation of the hydrogen recoils produced in the stopping foil. It is clear that, in ${}^4\text{He}$ -ERDA, a hydrogen-free stopping foil is essential to measure small quantities of hydrogen [19]. The Corteo simulations, made with exactly the same hydrogen concentrations, are very close to the simulations made with NDF. As in the previous example, they are slightly larger.

Finally, data collected from one InN sample using the Al stopping foil is shown in Fig. 5. Full experimental details are given elsewhere [20,21]. The angle dependent cross section for ${}^1\text{H}$ on N was taken from [22]. Again, the simulations made with both NDF and Corteo that assume no hydrogen is present in the sub-surface layer are one order of magnitude smaller than the observed data. Adjusting the hydrogen concentration in the bulk until the background calculated with NDF has the same integrated area as the data, we can determine that the hydrogen concentration is 0.17 at.%. The determination of such small values is relevant, because the free electron carrier concentration in unintentionally doped InN scales with the bulk hydrogen concentration [20].

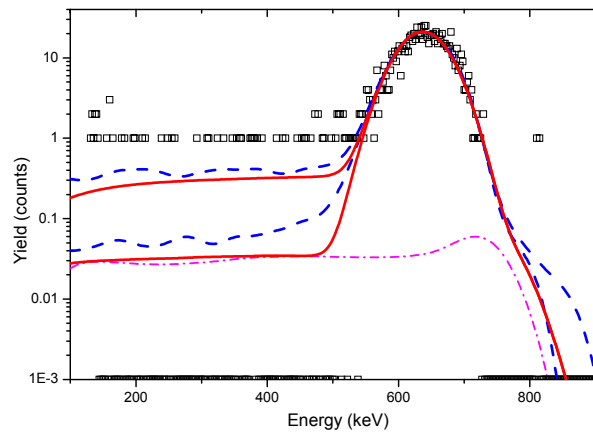


FIGURE 5. Data collected from an InN sample. The solid lines are calculated with NDF, and the dashed lines with Corteo. The lower lines assume that hydrogen is only present in the surface. The upper lines include 0.17 at.% hydrogen in the bulk.

SUMMARY

We developed an analytical algorithm to calculate the contribution of double scattering events in ERDA spectra. The model includes events where the primary ion first scatters off any of the target atoms, then produces a recoil, and events where the recoil is produced in the first scattering event, and then is scattered off any of the target atoms before being detected. The angular dependence of non-Rutherford cross sections is taken into account whenever the necessary data are available. Comparisons with Monte Carlo calculations show that the analytical calculations underestimate the low energy background by a factor up to 2, which is due to multiple scattering events not included in the analytical calculation.

We applied the code to measurements of hydrogen in Si made with an Al and a Kapton stopping foil. For the Kapton stopping foil the sensitivity to the hydrogen content of sub-surface layers is poor. For the Al stopping foil the sensitivity is much improved, and strong limits on the maximum hydrogen bulk content can be established. Finally, we show that small concentrations of hydrogen in InN can be determined with good accuracy using a standard ERDA set-up with a 2 MeV ^4He beam.

ACKNOWLEDGMENTS

NPB would like to thank the International Atomic Energy Agency for support under Research Contract No. 14365, Dr François Schietekatte for useful discussions on Monte Carlo calculations, and the four at Praia da Foz for strong encouragement to continue to work.

REFERENCES

1. P. Bauer, E. Steinbauer, J.P. Biersack, *Nucl. Instrum. Methods B* **64**, 711 (1992).
2. N.P. Barradas, et al., *Nucl. Instrum. Methods B* **262**, 281 (2007)
3. K. Arstila, T. Sajavaara, J. Keinonen, *Nucl. Instrum. Methods B* **174**, 163 (2001).
4. R.D. Franich, P.N. Johnston, I.F. Bubb, *Nucl. Instrum. Methods B* **219-220**, 87 (2004).
5. R.D. Franich, P.N. Johnston, I.F. Bubb, N. Dytlewski, D. D. Cohen *Nucl. Instrum. Methods B* **190**, 252 (2002).
6. F. Schietekatte, *Nucl. Instrum. Methods B* **266**, 1880 (2008).
7. S. Giangrandi, K. Arstila, B. Brijs, T. Sajavaara, A. Vantomme, W. Vandervorst, *Nucl. Instrum. Methods B* **257**, 1936 (2009).
8. N.P. Barradas, *Nucl. Instrum. Methods B* **225**, 318 (2004).
9. N.P. Barradas, C. Jeunes, and M.A. Harry, *Nucl. Instrum. Methods B* **136-138**, 1163 (1998).
10. N.P. Barradas, C. Jeunes, K.P. Homewood, B.J. Sealy, and M. Milosavljevic, *Nucl. Instrum. Methods B* **139**, 235 (1998).
11. A. Weber, H. Mommsen, W. Sarter, A. Weller, *Nucl. Instrum. Methods* **198**, 527 (1982).
12. H. H. Andersen, F. Besenbacher, P. Loftager, W. Möller, *Phys. Rev. A* **21**, 1891 (1980).
13. W. Eckstein, M. Mayer, *Nucl. Instrum. Methods B* **153**, 337 (1999).
14. F. Repplinger, J. P. Stoquert, P. Siffert, *Nucl. Instrum. Methods B* **80/81**, 24 (1993).
15. Ion Beam Analysis Nuclear Data Library, which also hosts the SigmaCalc code by Prof. A. F. Gurbich. <http://www-nds.iaea.org/ibandl/>
16. A.F. Gurbich, *Nucl. Instrum. Methods B* **268**, 1703 (2010).
17. A.F. Gurbich, *Nucl. Instrum. Methods B* **145**, 578 (1998).
18. H.R. Worthington, J.N. McGruer, D.E. Findley, *Physical Review* **90**, 899 (1953).
19. A. Tripathi, O. Kruse, H.D. Carstanjen, *Nucl. Instrum. Methods B* **219-220**, 435 (2004).
20. V. Darakchieva, et al., *Appl. Phys. Lett.* **96**, 081907 (2010).
21. K. Lorenz, N. P. Barradas, E. Alves, F. Munnik, Y. Nanishi, W. J. Schaff, L.W. Tu, V. Darakchieva, these proceedings.
22. I. Bogdanović Radović, Z. Siketić, M. Jaksic, A.F. Gurbich, *J. Appl. Phys.* **104**, 074905 (2008).